

Response of primary production and calcification to changes of $p\text{CO}_2$ during experimental blooms of the coccolithophorid *Emiliana huxleyi*

Bruno Delille,¹ Jérôme Harlay,² Ingrid Zondervan,³ Stephan Jacquet,⁴ Lei Chou,² Roland Wollast,^{2,5} Richard G. J. Bellerby,⁶ Michel Frankignoulle,^{1,7} Alberto Vieira Borges,¹ Ulf Riebesell,⁸ and Jean-Pierre Gattuso⁹

Received 17 June 2004; revised 25 February 2005; accepted 6 April 2005; published 2 June 2005.

[1] Primary production and calcification in response to different partial pressures of CO_2 (PCO_2) (“glacial,” “present,” and “year 2100” atmospheric CO_2 concentrations) were investigated during a mesocosm bloom dominated by the coccolithophorid *Emiliana huxleyi*. The day-to-day dynamics of net community production (NCP) and net community calcification (NCC) were assessed during the bloom development and decline by monitoring dissolved inorganic carbon (DIC) and total alkalinity (TA), together with oxygen production and ^{14}C incorporation. When comparing year 2100 with glacial PCO_2 conditions we observed: (1) no conspicuous change of net community productivity (NCP_y); (2) a delay in the onset of calcification by 24 to 48 hours, reducing the duration of the calcifying phase in the course of the bloom; (3) a 40% decrease of NCC; and (4) enhanced loss of organic carbon from the water column. These results suggest a shift in the ratio of organic carbon to calcium carbonate production and vertical flux with rising atmospheric PCO_2 .

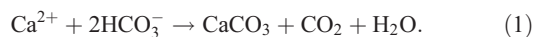
Citation: Delille, B., et al. (2005), Response of primary production and calcification to changes of $p\text{CO}_2$ during experimental blooms of the coccolithophorid *Emiliana huxleyi*, *Global Biogeochem. Cycles*, 19, GB2023, doi:10.1029/2004GB002318.

1. Introduction

[2] In the context of rising PCO_2 in the atmosphere and concomitant increase of $p\text{CO}_2$ in the oceans, the response of marine organisms and ecosystems to elevated $p\text{CO}_2$ has received little attention compared to terrestrial plants and ecosystems. This is partly due to the fact that photosynthesis by marine phototrophs is, generally, not considered to be carbon limited due to the large pool of DIC in seawater, mostly in the form of bicarbonate. Indeed, if some studies have shown that marine autotrophic communities are often insensitive to $p\text{CO}_2$ changes, several studies have shown that some seagrass [Zimmerman et al., 1997], macroalgae

[Gao et al., 1993], diatom [Riebesell et al., 1993; Chen and Durbin, 1994], coccolithophorid [Nimer and Merrett, 1993; Hiwatari et al., 1995; Riebesell et al., 2000; Zondervan et al., 2001], and cyanobacteria [Qiu and Gao, 2002] species exhibit higher rates of photosynthesis under CO_2 enrichment. In their review of the effects of CO_2 concentration on marine plankton, Wolf-Gladrow et al. [1999] pointed out the apparent discrepancy between ample CO_2 supply from the bulk medium combined with the capacity for direct utilization of HCO_3^- in many marine phytoplankton on the one hand and the sensitivity of both phytoplankton growth rate and elemental composition to CO_2 concentration on the other. They argue that one of the factors to be considered when trying to resolve this discrepancy is the low affinity for CO_2 of the primary carboxylating enzyme RuBisCO and that the sensitivity of marine phytoplankton to CO_2 is best viewed as a co-limitation of CO_2 in concert with light availability and other limiting factors such as nutrients. Irrespective of which mechanism is responsible for the sensitivity of some phytoplankton species to $p\text{CO}_2$, the topic has received comparatively little attention considering its potential importance for carbon export and sequestration and its potential negative feedback to rising atmospheric CO_2 .

[3] The response of calcifying organisms and communities to elevated $p\text{CO}_2$ appears to be more straightforward. Biogenic precipitation of calcium carbonate is generally described by the following equation:



¹Unité d’Océanographie Chimique, Interfaculty Center for Marine Research (MARE), Université de Liège, Liège, Belgium.

²Laboratoire d’Océanographie Chimique et Géo chimie des eaux, Université Libre de Bruxelles, Campus de la Plaine, Brussels, Belgium.

³Alfred Wegener Institute for Polar and Marine Research, Bremerhaven, Germany.

⁴Station INRA d’Hydrobiologie Lacustre, UMR 42 Cartell, CNRS, Thonon, France.

⁵Deceased on 28 July 2004.

⁶Bjerknes Centre for Climate Research, University of Bergen, Bergen, Norway.

⁷Deceased on 13 March 2005.

⁸Leibniz Institute for Marine Sciences, University of Kiel, Kiel, Germany.

⁹Laboratoire d’Océanographie de Villefranche, UMR 7093, CNRS, Université Pierre et Marie Curie, Villefranche-sur-mer, France.

[4] Thus calcification acts as a source of CO_2 to the water column and counteracts the photosynthetic uptake of CO_2 . The net effect of these two antagonistic processes on CO_2 is dependent on the ratio of NCC to NCP (C:P). Moreover, the release of CO_2 by NCC is modulated by the buffering capacity of the carbonate system [Frankignoulle, 1994]. Any variation of the C:P ratio will have significant implications on biogeochemical fluxes, and particularly on the sign and strength of the overall feedback of coccolithophorids to rising atmospheric PCO_2 . Furthermore, changes of the C:P ratio affect the density and sinking rate of coccolithophorid cells and debris and, therefore, the magnitude of carbon export. Hence Buitenhuis *et al.* [2001] suggested that a decrease of the C:P ratio induces a decrease of carbon export and affects the overall uptake of CO_2 by coccolithophorids.

[5] Generally, the rate of calcification decreases with rising $p\text{CO}_2$ and diminishing CaCO_3 saturation state (Ω). This response is nowadays well documented for reef-building corals and coralline algae [Gattuso *et al.*, 1999]. Mesocosm experiments have recently established the link between the decrease in calcification rate of coral reefs with rising CO_2 , and the concomitant drop of aragonite Ω [Langdon *et al.*, 2000; Leclercq *et al.*, 2002; Langdon *et al.*, 2003]. In the same way, Bijma *et al.* [1999] observed that the decrease of Ω causes a decrease in the calcification rate by foraminifera. Riebesell *et al.* [2000] and Zondervan *et al.* [2001, 2002] observed a similar response with coccolithophorids, which may be the largest contributors to marine pelagic calcification. These authors showed, in batch cultures of *Emiliania huxleyi* and *Gephyrocapsa oceanica*, that the production of particulate organic carbon (POC) increases with increasing CO_2 and is additionally depending on the total irradiance and the photoperiod length. Also, the production of particulate inorganic carbon (PIC) decreases, leading to the decrease of the C:P ratio. It therefore seems that depression of calcification or/and C:P ratio at elevated $p\text{CO}_2$ is a general feature among marine calcifying organisms.

[6] Previous studies of the response of coccolithophorids to increasing $p\text{CO}_2$ were most often made in batch cultures by manipulating the carbonate system through the addition of acid or base [Nimer and Merrett, 1993; Buitenhuis *et al.*, 1999; Zondervan *et al.*, 2001, 2002]. The aim of identifying the influence of increasing CO_2 on calcification has driven these authors to eliminate environmental interactions and to grow cultures under optimal conditions which do not perfectly reflect in situ conditions. Furthermore, the manipulation of the carbonate system through the addition of acid and base also alters TA, whereas oceanic TA will not change significantly in the next decades. For instance, an increase of $p\text{CO}_2$ induced by acid addition leads to a decrease in calcite and aragonite saturation states 20% higher and an increase in HCO_3^- concentration 60% lower than would be observed for the same increase of $p\text{CO}_2$ induced by CO_2 addition. However, calcification appears to be controlled by Ω than by $p\text{CO}_2$ per se [Langdon *et al.*, 2000; Leclercq *et al.*, 2002]. Moreover, HCO_3^- was suggested to be the substrate for calcification of *E. huxleyi* [Buitenhuis *et al.*, 1999]. Therefore the control of the carbonate system using gas addition may be more suited to reproduce the future

changes of carbonate chemistry than acid/base addition techniques.

[7] Building on the pioneering batch culture experiments, the aim of the present study was to follow the development and decline of a bloom of a natural plankton community dominated by the coccolithophorid *E. huxleyi* exposed to various $p\text{CO}_2$ under more natural conditions in large seawater volumes. This allowed us to investigate the $p\text{CO}_2$ related effects at the community level and to examine their impacts on the dynamics of the bloom. This was achieved by employing large seawater enclosures containing natural assemblages of bacterioplankton, phytoplankton, and micro-zooplankton kept under ambient light and temperature conditions and subjected to atmospheric CO_2 concentrations simulating the “glacial,” “present,” and “year 2100” atmospheric PCO_2 conditions (respectively, 180, 370, and 700 ppmV). Inorganic nutrient concentrations and the carbonate chemistry were adjusted prior to the onset of the bloom, and were allowed to evolve without further regulation as would occur in the mixed surface layer of a stratified water column during the course of a bloom. The day-to-day response of inorganic and organic carbon production by the enclosed communities was assessed using O_2 production and ^{14}C uptake during incubations together with the monitoring of daily changes in TA and DIC.

2. Material and Methods

2.1. Overall Description of the Experiment

[8] The experiment was carried out between 31 May and 25 June 2001 at the Marine Biological Field Station (Raunefjorden, 60.3°N, 5.2°E) of the University of Bergen, Norway. Nine enclosures made of polyethylene bags of 2 m diameter and volume of 11 m³ were used. The bags were secured to the sides of a raft equipped with a small laboratory. Each bag was filled with unfiltered nutrient poor (post-spring bloom) water pumped at a depth of 2 m in the fjord on 1 June. The following provides a short description of the experimental setup, for more details we refer to a companion paper by Engel *et al.* [2004a].

[9] The tops of the mesocosms were covered with tetrafluoroethylene films (95% transmission for photosynthetically active radiation) forming a tent over more than 90% of the mesocosm surface area. The atmospheric PCO_2 underneath the tents was controlled by injecting a continuous stream of gases with a known CO_2 content. Three levels of $p\text{CO}_2$ (180, 370, and 700 ppmV) were used with three replicates each; they will be referred to as glacial (Mesocosm (M)7, M8, and M9), present (M4, M5, and M6) and year 2100 (according to the Intergovernmental Panel on Climate Change “business as usual” scenario IS92a; M1, M2, and M3). In contrast to similar laboratory experiments carried out on phytoplankton cultures, in which seawater $p\text{CO}_2$ was maintained at constant values throughout the experiment, in this study, seawater CO_2 was manipulated only at the start of the experiment before initiation of the bloom. This was achieved by bubbling CO_2 -free, ambient, or CO_2 -enriched air at the bottom of the mesocosms until 6 June (hereinafter referred to as “day 0”). From day 0 until the end of the experiment, the carbonate system was

Table 1. The $p\text{CO}_2$ (ppmV) and Concentration of CO_2 ($\mu\text{mol kg}^{-1}$) of Each Mesocosm at d_0 , d_{10} , and d_{15}

Mesocosm	d_0		d_{10}		d_{15}	
	$p\text{CO}_2$, ppmV	$[\text{CO}_2]$, $\mu\text{mol kg}^{-1}$	$p\text{CO}_2$, ppmV	$[\text{CO}_2]$, $\mu\text{mol kg}^{-1}$	$p\text{CO}_2$, ppmV	$[\text{CO}_2]$, $\mu\text{mol kg}^{-1}$
<i>Year 2100</i>						
M1	710	31.7	542	23.1	293	12.3
M2	709	31.6	557	23.8	323	13.6
M3	720	32.1	604	25.1	317	13.3
<i>Present</i>						
M4	407	18.2	360	15.4	217	9.1
M5	426	19.1	344	14.7	228	9.7
M6	408	18.3	341	14.5	205	8.6
<i>Glacial</i>						
M7	188	8.4	176	7.5	118	4.9
M8	192	8.6	185	7.9	125	5.3
M9	190	8.5	185	7.9	128	5.4

allowed to evolve naturally while maintaining only the atmosphere underneath the tents covering each mesocosm at glacial, present, and year 2100 atmospheric $p\text{CO}_2$ conditions. The seawater $p\text{CO}_2$ values reached on 6 June are given in Table 1. To promote the development of the coccolithophorid bloom, nitrate and phosphate were added to each mesocosm on day 0 at initial concentrations of about $17 \mu\text{mol L}^{-1} \text{NO}_3^-$ and $0.5 \mu\text{mol L}^{-1} \text{PO}_4^{3-}$. The water enclosed in the mesocosms was gently homogenized using an airlift system consisting of a plastic tube in which a gas stream, having a $p\text{CO}_2$ identical to that of the atmosphere confined above the mesocosm, produced an upward motion of water in the tube. The flow rate was very low in order to avoid significant gas exchange between the air stream and seawater.

[10] Each mesocosm was sampled every day between 0900 and 1100 local time (LT), while daylight lasted from around 0430 to 2300 LT, to measure the abundances of various phytoplankton groups, bacteria, and viruses and the concentration of nutrients, as well as parameters of the carbonate system (TA and $p\text{CO}_2$). Elapsed time is referred to as “ d_x ” where x is the number of days since “ d_0 ”.

2.2. Seawater Partial Pressure of CO_2 and Temperature

[11] Measurements of $p\text{CO}_2$ were carried out using an equilibrator coupled to an infrared gas analyzer (IRGA, Li-Cor® 6262). Seawater flows into the equilibrator (3 L min^{-1}) from the top, and a closed air loop (3 L min^{-1}) ensures circulation through the equilibrator (from the bottom to the top), a desiccant (Drierite®), and the IRGA [Frankignoulle *et al.*, 2001]. The barometric pressure inside the equilibrator was kept equal to atmospheric pressure. Both the barometric pressure and temperature were monitored in the air loop. The IRGA was calibrated daily with air standards with nominal mixing ratios of 0, 350, and $800 \pm 0.3 \text{ ppmV}$ of CO_2 supplied by Air Liquide Belgium® and Hydrogas®. The equilibration time of the system was less than 3 min [Frankignoulle *et al.*, 2001]. The system was kept running twice this time before recording and averaging the values given by the IRGA and temperature sensors over a 30-s period.

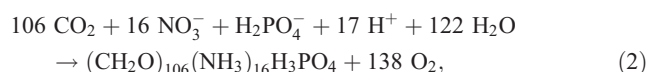
[12] In situ and equilibrator temperatures were measured simultaneously using Li-Cor® sensors. Differences in temperature were less than 0.5°C . TA measurements were made with each measurement of $p\text{CO}_2$ and used to temperature correct $p\text{CO}_2$ using dissociation constants of Roy *et al.* [1993]. The uncertainty of $p\text{CO}_2$ is estimated to $\pm 3 \text{ ppmV}$.

2.3. Total Alkalinity, Dissolved Inorganic Carbon, and Salinity

[13] TA was measured using the classical Gran potentiometric method [Gran, 1952] on 100-mL GF/C filtered samples. The reproducibility of measurements was $\pm 3 \mu\text{mol kg}^{-1}$.

[14] Dissolved inorganic carbon (DIC) was calculated from $p\text{CO}_2$ and TA. CO_2 speciation was calculated using the CO2SYS Package [Lewis and Wallace, 1998], the CO_2 acidity constants of Roy *et al.* [1993], the CO_2 solubility coefficient of Weiss [1974], and the borate acidity constant of Dickson [1990]. The total borate molality was calculated using the Uppström [1974] boron to salinity ratio. The uncertainty on the DIC computation is estimated to $\pm 5 \mu\text{mol kg}^{-1}$.

[15] TA was corrected for the drawdown of nitrate and phosphate associated with phytoplankton nutrient utilization. According to the classical Redfield-Ketchum-Richards reaction of biosynthesis [Redfield *et al.*, 1963; Richards, 1965],



1 mole of H^+ is consumed for each mole of NO_3^- or H_2PO_4^- consumed through biosynthesis, increasing TA by 1 mole. TA corrected for primary production ($\text{TA}_{\text{corrected}}$) can therefore be computed from measured TA ($\text{TA}_{\text{measured}}$) using the relation

$$\text{TA}_{\text{corrected}} = \text{TA}_{\text{measured}} - \Delta\text{NO}_3^- - \Delta\text{H}_2\text{PO}_4^-, \quad (3)$$

where ΔNO_3^- and $\Delta\text{H}_2\text{PO}_4^-$ denote the decreases of NO_3^- and H_2PO_4^- since the reference day (d_1). Correction for nutrient uptake accounts for less than 13% of the TA changes.

[16] DIC changes were corrected daily for air-sea exchange of CO_2 using the air-sea gradient of CO_2 , the volume of the bags, and assuming that water in the bags was well homogenized and that there was zero wind under the tents. Air-sea exchange of CO_2 from the enclosed atmosphere to the water was computed using the algorithm for stagnant boundary layer thickness from Smith [1985], molecular diffusivity from Jähne *et al.* [1987], and chemical enhancement model from Hoover and Berkshire [1969]. The formulation given by Smith [1985] was established using the stagnant film model and measurements from wind tunnels at low wind speed and corresponds better to our experimental setup than other relations derived from in situ measurements affected by additional turbulent processes such as currents and rain. Correction for air-sea exchange accounted for less than 5% of changes in DIC.

[17] Normalized TA and DIC at a constant salinity ($S = 31$) are denoted as TA_{31} and DIC_{31} . Salinity was measured using a conductivity-temperature-pressure sensor (CTD SAIV A/S, model SD204).

2.4. Flow Cytometry Sample Processing and Analysis

[18] Analyses were performed with a FACSCalibur flow cytometer (Becton Dickinson®) equipped with an air-cooled laser providing 15 mW at 488 nm and with standard filter setup. The algae were analyzed from fresh samples at a high flow rate ($\sim 70 \mu\text{L min}^{-1}$) with the addition of $1 \mu\text{m}$ fluorescent beads (Molecular Probes®). Autotrophic groups were discriminated on the basis of their forward or right angle light scatter (FALS, RALS) and chlorophyll (and phycoerythrin for *Synechococcus* and cryptophyte populations) fluorescence. Enumeration of viruses was carried out on samples fixed with glutaraldehyde (0.5% final concentration) and frozen (in liquid nitrogen). Once thawed at 37°C , samples were diluted 10 to 100 times in Tris-EDTA ($\text{pH} = 8$) buffer and heated for 10 min at 80°C after staining with the DNA dye SYBR® Green I (1/20,000 final concentration, Molecular Probes®, [Marie et al., 1999]). Counts were performed at medium rate ($\sim 30 \mu\text{L min}^{-1}$). Viruses were discriminated on the basis of their RALS versus green DNA-dye fluorescence. Listmode files were analyzed using CYTOWIN [Vaulot, 1989] (available at <http://www.sb-roscoff.fr/Phyto/cyto.html#cytowin>) and WinMDI (version 2.7, Trotter, available at <http://www.bio.umass.edu/mcbfac/flowcat.html#winmdi>).

2.5. Primary Production From ^{14}C Incubations

[19] Subsurface seawater for incubation experiments was sampled in M1, M4, and M9 before sunrise. All water samples were pre-sieved through a $200\text{-}\mu\text{m}$ nylon mesh to remove large zooplankton. All incubations were carried out in 60-mL flasks inoculated with H^{14}CO_3 ($\sim 20 \mu\text{Ci}$ per 500 mL) and incubated in situ for 24 hours at a depth of 1.5 m in the water of the fjord adjacent to the mesocosms. Concomitant incubations were made in dark bottles. After incubation, samples were filtered on Whatman® GF/F filters under gentle vacuum. Duplicate filters were collected for each sample incubated and rinsed with 0.2-m-filtered seawater in order to remove excess DI^{14}C . One set of filters was treated with $100 \mu\text{L HCl}$ (0.01 N) to eliminate the radiocarbon incorporated into CaCO_3 . Primary production was estimated from ^{14}C measurements after exposure of the filters to HCl while calcification was estimated by subtracting primary production from the total ^{14}C collected on untreated filters.

2.6. Net Community Production and Respiration (O_2 Technique)

[20] Samples were collected in mesocosms M1, M2, M4, M5, M8, and M9 before sunrise and immediately distributed into 60-mL BOD bottles (overflowing $> 150 \text{ mL}$). For each sampled mesocosm, four bottles were fixed immediately with Winkler reagents, three sets of three bottles were incubated in situ nearby the mesocosms at 0.5, 1.5, and 4 m, and four bottles were incubated in the laboratory in darkness at in situ temperature. The bottles incubated in situ were fixed at sunset, and duration of the incubations was

about 18 hours (from about 0510 LT until 2300 LT). The dark bottles incubated in the laboratory were fixed the next day between 0800 and 1000 LT, and the duration of the incubations was 27 to 29 hours.

[21] The concentration of dissolved oxygen was determined using an automated Winkler titration technique with a potentiometric end-point detection [Anderson et al., 1992] using an Orion® 9778-SC electrode. Reagents and standardizations were similar to those described by Knap et al. [1994].

2.7. Net Community Production and Net Community Calcification From DIC and TA Changes

[22] NCC can be estimated from the time course of $\text{TA}_{\text{corrected}}$ according to

$$\text{NCC} = -0.5 \times \frac{\Delta\text{TA}_{\text{corrected}}}{\Delta t}, \quad (4)$$

where Δt denotes elapsed time. Similarly, net community production (NCP_{DIC}) of organic carbon can be computed from changes in DIC and TA according to

$$\text{NCP}_{\text{DIC}} = -\frac{\Delta\text{DIC}}{\Delta t} + 0.5 \times \frac{\Delta\text{TA}_{\text{corrected}}}{\Delta t}. \quad (5)$$

3. Results

3.1. *E. Huxleyi* Abundance, $p\text{CO}_2$, DIC_{31} , and TA_{31}

[23] A succession of distinct phytoplankton assemblages took place in the course of the experiment. The assemblage was first dominated by *Synechococcus* sp. and nanoflagellates (S. Jacquet, unpublished data, 2001), and subsequently by *E. huxleyi* [Engel et al., 2004a]. From d_0 to d_7 , both *Synechococcus* sp. and nanoflagellate abundances increased to reach a maximum between d_5 and d_7 , depending on the mesocosm, with abundances ranging from 10 to $15 \times 10^3 \text{ cells mL}^{-1}$ and 30 to $170 \times 10^3 \text{ cells mL}^{-1}$ for *Synechococcus* sp. and nanoflagellates, respectively (S. Jacquet, unpublished data, 2001). This maximum cell abundance corresponded to chlorophyll-*a* (Chl *a*) concentrations ranging from 0.3 to $0.5 \mu\text{g L}^{-1}$ [Engel et al., 2004a]. The abundance of *Synechococcus* sp. and nanoflagellates subsequently decreased sharply to less than 3.2 and $7.0 \times 10^3 \text{ cell mL}^{-1}$, respectively on d_{10} , while *E. huxleyi* abundance remained below $2.7 \times 10^3 \text{ cell mL}^{-1}$ from d_0 to d_{10} (Figure 1). During this coccolithophorid pre-bloom phase, small decreases of DIC_{31} and PCO_2 were observed while TA_{31} remained unchanged with similar values in all mesocosms.

[24] On d_{10} , the decreases of DIC_{31} and $p\text{CO}_2$ were larger and concomitant with the sharp increase of the abundance of *E. huxleyi*. The minimum $p\text{CO}_2$ was observed on d_{16} . The magnitude of changes in $p\text{CO}_2$ exhibited large differences depending on the $p\text{CO}_2$ conditions from d_0 to d_{14} ranging from $386 \pm 16 \text{ ppmV}$ in the year 2100 mesocosms to $187 \pm 13 \text{ ppmV}$ in the present mesocosms and $61 \pm 2 \text{ ppmV}$ in the glacial mesocosms. However, until d_{14} , the differences in DIC_{31} patterns between mesocosms were not significant. From d_{12} onward, TA_{31} decreased sharply in all mesocosms indicating the onset of calcification by coccolithophorids.

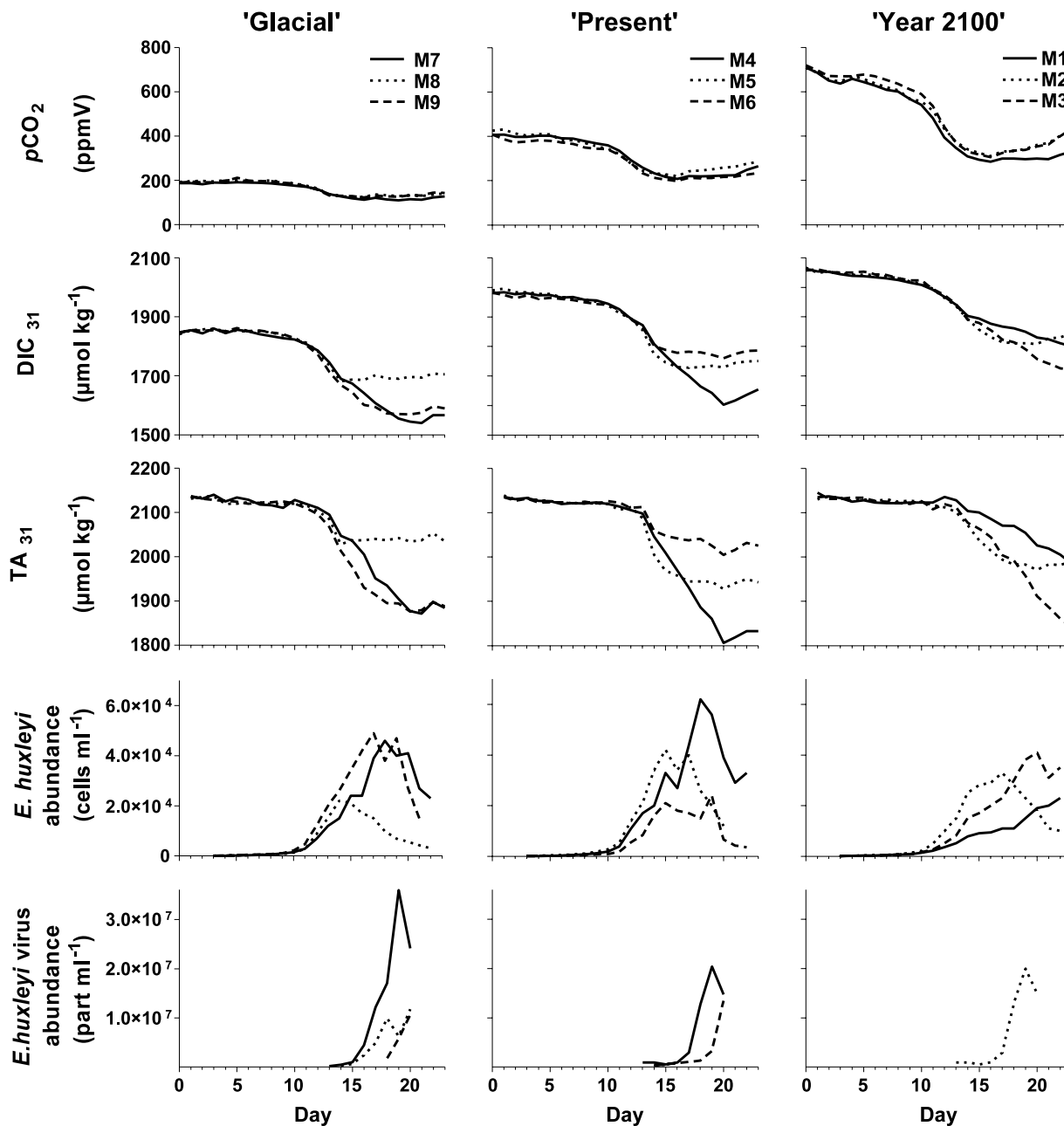


Figure 1. Evolution of seawater $p\text{CO}_2$, DIC, TA, abundance of *Emiliana huxleyi*, and virus specific for *E. huxleyi* in the nine mesocosms. TA (corrected for the uptake of NO_3^- and PO_4^{3-}) and DIC are normalized to a constant salinity of 31.

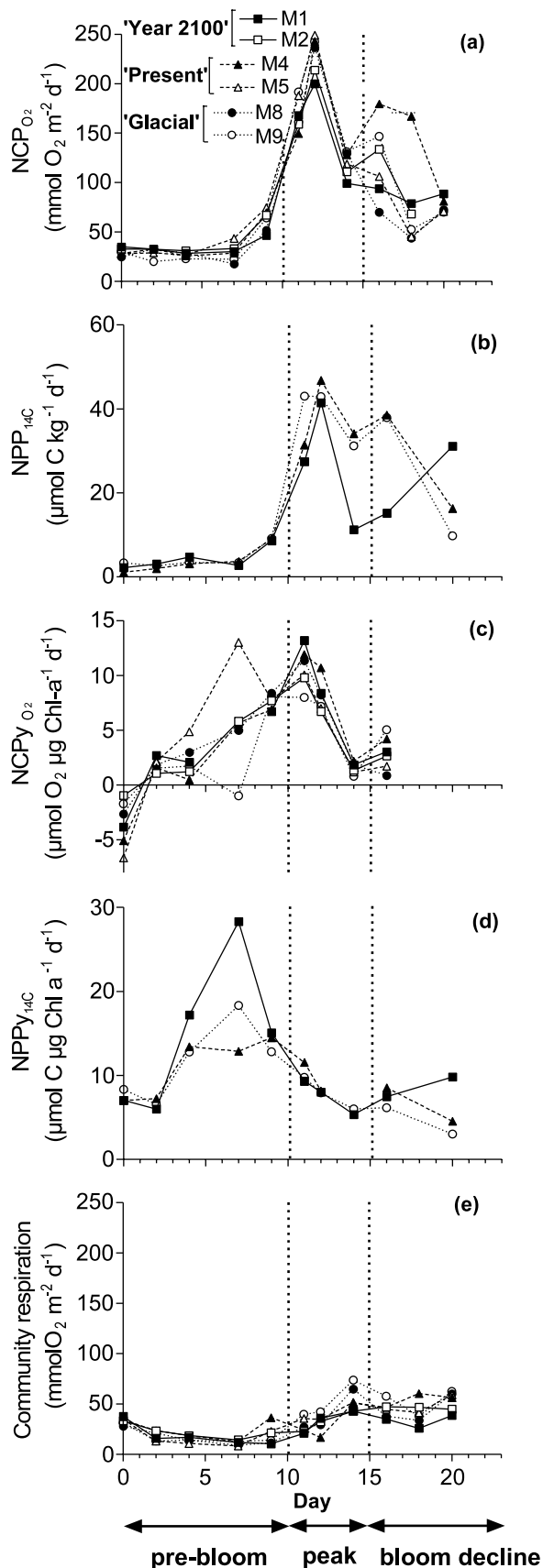
Decreases of TA_{31} ranged from 30 to $95 \mu\text{mol kg}^{-1}$ between d_{13} and d_{14} .

[25] Between d_{14} and d_{16} , the overall patterns of most parameters indicate the transition toward the decline of the bloom. On d_{14} , nutrients (NO_3^- and PO_4^{3-}) were exhausted in all mesocosms [Engel et al., 2004a]. From d_{16} onwards, $p\text{CO}_2$ remained constant or increased slightly whereas DIC_{31} continued to decrease in most mesocosms.

[26] DIC_{31} evolutions became confusing after d_{14} . DIC_{31} reached rapidly a plateau on d_{14} in M5, M6 and M8 (glacial mesocosm) whereas it continued to decrease significantly in M1 and M3, M4, M7, and M9 (year 2100 mesocosms).

Concomitantly, TA_{31} also began to differ greatly between mesocosms. In most cases, TA_{31} reached a plateau after a large and continuous drop. However, it should be noted that TA_{31} decreased at a high rate until the end of the experiment in M1 and M3 (year 2100 conditions).

[27] Interestingly, within these two mesocosms, viruses specific to *E. huxleyi* were either absent or present in low abundance. The collapse of nutrient-induced *E. huxleyi* blooms, as we observed in 7 of the 9 mesocosms, has also been commonly reported in similar experiments. It has been attributed to viral lysis by a virus identified as *EhV* [Bratbak et al., 1996; Jacquet et al., 2002; Castberg et al., 2001]



which belongs to the genus *Coccolithovirus* proposed by Schroeder *et al.* [2002] within the family of algal viruses *Phycodnaviridae*.

3.2. Net Community Production of Organic Carbon

[28] NCP (Figure 2a) assessed from oxygen incubations (NCP_{O_2}) and NCP_{O_2} normalized against Chl *a* concentrations (Figure 2c), i.e., the net community productivity (NCPy_{O_2}), exhibited similar patterns for all the mesocosms during the pre-bloom period (d_0 to d_{10}) and the peak of the bloom (d_{10} to d_{15}). They increased sharply from d_7 onward to reach maximum values on d_{12} coinciding with the marked increase of abundance of *E. huxleyi* (Figure 1). From d_{16} onward, mesocosms showed different NCP_{O_2} patterns which do not seem to be related to PCO_2 conditions.

[29] Net primary production (Figure 2b) estimated by the uptake of ^{14}C ($\text{NPP}_{14\text{C}}$) exhibited a similar pattern to those of NCP_{O_2} . From d_{14} onward, $\text{NPP}_{14\text{C}}$ appears to be lower in M1 (year 2100) compared to M4 (present) and M9 (glacial). However, similarly to NCPy_{O_2} , $\text{NPPy}_{14\text{C}}$ (Figure 2d) was similar in all the mesocosms from d_9 onward.

[30] Community respiration (Figure 2e) assessed from oxygen incubations decreased during the pre-bloom period, then increased during the peak of the bloom to reach a maximum value ranging from 40 to 75 $\text{mmol O}_2 \text{ m}^{-2} \text{ d}^{-1}$ on d_{14} . It subsequently remained between 30 and 60 $\text{mmol O}_2 \text{ m}^{-2} \text{ d}^{-1}$. No obvious differences of community respiration were found in the various PCO_2 conditions.

3.3. $\text{Ca}^{14}\text{CO}_3$ Production Rate

[31] Calcification by *E. huxleyi* estimated from ^{14}C in situ incubations started on d_9 in M4 and M9 and on d_{11} in M1 (Figure 3a), suggesting that the onset of calcification was delayed under year 2100 PCO_2 conditions. The highest values were reached on d_{13} in M4 and M9 (16 and 20 $\mu\text{mol CaCO}_3 \text{ kg}^{-1} \text{ d}^{-1}$, respectively). Calcification was higher in M9 than in M4, while it remained low in M1. This is consistent with the larger decreases of TA_{31} observed in M4 and M9 compared to M1. During the peak of the bloom, M1 exhibited lower rates of calcification normalized to Chl *a* than M4 and M9 (Figure 3b), suggesting a lower competence of *E. huxleyi* to calcify under year 2100 PCO_2 conditions, while net primary productivity seemed unaffected (see section 3.2).

3.4. Molar Respiration Ratio

[32] We compared net community production values obtained from O_2 incubations with values estimated from

Figure 2. (a) Net community production estimated from oxygen incubations (NCP_{O_2}), (b) net primary production estimated from ^{14}C incubations ($\text{NPP}_{14\text{C}}$), (c) net community production normalized against chlorophyll *a* from oxygen incubations (NCPy_{O_2}), (d) net primary production normalized against chlorophyll *a* from ^{14}C ($\text{NPPy}_{14\text{C}}$), and (e) community respiration (CR) based on oxygen incubations in mesocosms 1 (solid squares, solid line), 2 (open squares, solid line), 4 (solid triangles, dashed line), 5 (open triangles, dashed line), 8 (solid circles, dotted line), and 9 (open circles, dotted line).

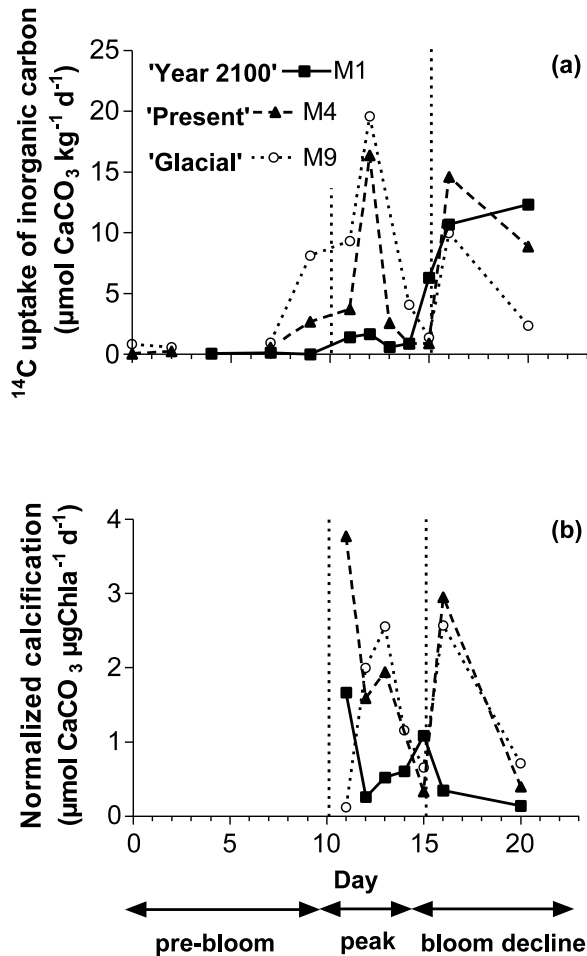


Figure 3. ^{14}C uptake of (a) inorganic carbon and (b) normalized calcification in mesocosms 1 (squares, solid line), 4 (dashed line), and 9 (triangles, dotted line).

DIC and TA changes by plotting NCP_{O_2} versus NCP_{DIC} (Figure 4). Model II linear regression gives a slope of 1.45 ± 0.12 and a correlation coefficient of 0.68 ($p < 0.0001$, $n = 54$, 4). The slope of the linear regression corresponds to the so-called molar respiration ratio (R.R.). Indeed, if we consider the respiration as the reverse of the Redfield-Ketchum-Richard equation (equation (2)), the complete oxidic degradation of phytoplankton theoretically requires 138 moles of dissolved O_2 /106 moles of organic carbon (C) leading to a molar respiration ratio (O_2/C) of 1.30. The R.R. obtained in the present study agrees well with the estimates of Hedges *et al.* [2002] based on phytoplankton elemental composition using nuclear magnetic resonance which ranges from 1.41 to 1.47, depending on the geographic area considered. The consistency of these results validates the use of NCP_{DIC} derived from DIC and TA and enables therefore a comprehensive day-to-day comparison of NCP and NCC.

3.5. Timing of Organic and Inorganic Carbon Production

[33] NCP_{DIC} as a function of NCC are shown in the Figure 4 where each point corresponds to a daily measure-

ment. Connecting day-to-day estimates provides an overview of the temporal evolution of NCP_{DIC} relative to NCC. During the pre-bloom period, NCP_{DIC} increased steadily (upward displacement along the Y-axis), first owing to the rising abundances of *Synechococcus* sp. and nano-flagellates, and subsequently to the onset of the bloom of *E. huxleyi*. The increase of NCP_{DIC} was enhanced from d_{10} onward in all the conditions, concomitantly with the beginning of the peak of the bloom period (Figure 1) and leads to maximum values of NCP_{DIC} on d_{12} and d_{13} . By d_{15} the nutrients were exhausted; NCP_{DIC} decreased markedly. NCC increases (displacement to the right along the X-axis) in a second phase, when the coccolithophorid bloom is well underway, proceeded from d_{11} to d_{19} , and remained at a high level while NCP_{DIC} decreased dramatically, which is consistent with observations in cultures of *E. huxleyi* [Dong *et al.*, 1993]. The third phase was the collapse of the bloom with a dramatic decrease of both NCP_{DIC} and NCC. This phase corresponds to the period during which the coccolithovirus abundance passes over a threshold value, estimated to be around $5 \cdot 10^6$ part mL^{-1} (dashed lines in Figure 5). At the end of the experiment, NCP_{DIC} and NCC show negative values due to elevated respiration and CaCO_3 dissolution, as suggested by Milliman *et al.* [1999]. This is consistent with the increase of both CR (Figure 2c) and bacterial abundance determined by flow cytometry (S. Jacquet, unpublished data, 2001).

[34] Under glacial conditions (M7, M8 and M9), NCC started at the onset of the peak of the bloom (d_{10} – d_{11}) and then increased steadily in parallel to NCP_{DIC} leading to an almost simultaneous maximum (only 1 day time lag). In contrast, in the year 2100 conditions (M1, M2 and M3), NCC began later (d_{12} to d_{13}), and suddenly, while NCP_{DIC} had already reached its maximum. NCC subsequently increased very rapidly while NCP_{DIC} was decreasing. The present conditions exhibited an intermediate behavior between the year 2100 and glacial conditions: The maximum level of NCP_{DIC} was reached when NCC was

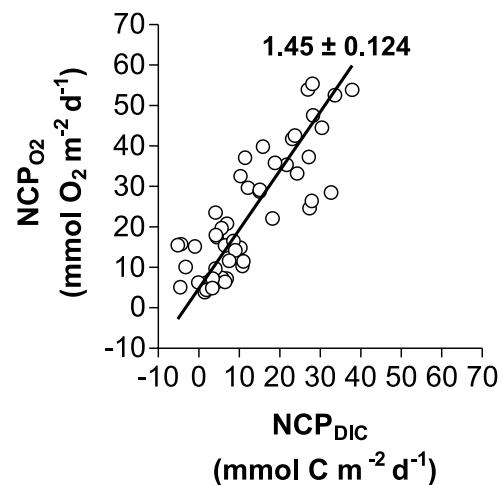


Figure 4. Net community production computed from oxygen incubation (NCP_{O_2}) versus NCP computed from DIC and TA (NCP_{DIC}) with a model II regression line.

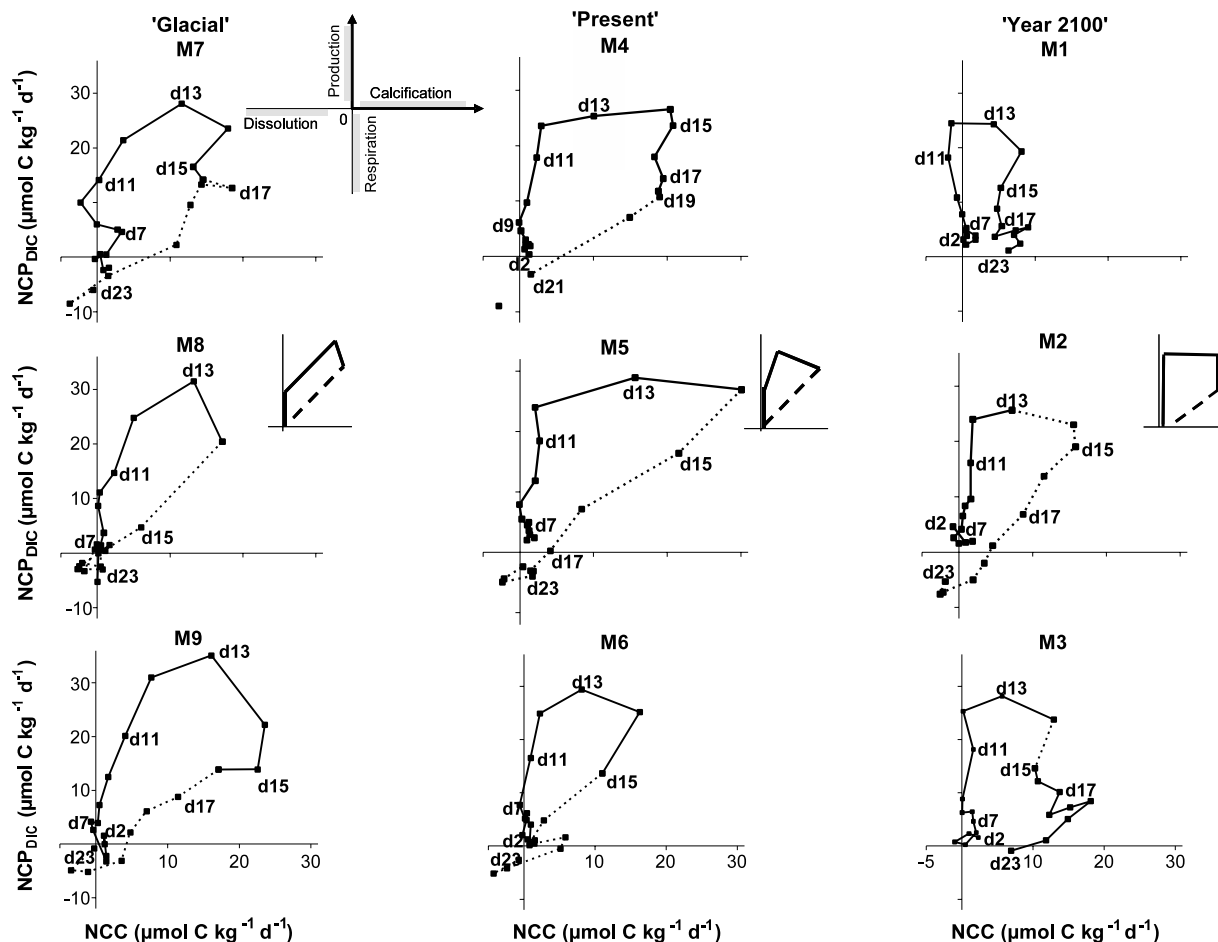


Figure 5. Hysteresis showing the changes of net community production (NCP_{DIC}) and calcification (NCC) during the experiment. NCP_{DIC} is plotted versus NCC, and each data point corresponds to 1 day. Positive and negative Y-axis values indicate, respectively, a net gain and loss of organic carbon. Positive and negative X-axis values indicate, respectively, net production and dissolution of calcium carbonate. Time is running clockwise, and dates of some points are indicated (“d_x”). Dashed lines indicate when the *E. huxleyi* virus (*EhV*) abundance was above $5 \times 10^6 \text{ part mL}^{-1}$. A schematic shape is provided for each condition.

already substantial but had not reached its maximum value.

[35] Thus, if the overall pattern of NCP_{DIC} prior to viral lysis is similar for all the conditions, the onset of NCC occurs sooner in the glacial and present conditions than in the year 2100 conditions. This is consistent with the calcification rates measured with the ^{14}C in situ incubations. Furthermore, under glacial conditions, NCC increases steadily from the very beginning of the peak of the bloom in parallel to the exponential rise of NCP_{DIC} , while in the year 2100, NCC occurs suddenly at the maximum of NCP_{DIC} .

3.6. Mean Community Production and Calcification Rates

[36] Changes in the standing stocks of total organic carbon (TOC) and PIC, associated with the bloom of *E. huxleyi*, were assessed during the peak of the bloom

(d₁₀–d₁₅) by integrating, respectively, daily NCP_{DIC} and NCC over time (Figure 6). TOC standing stocks exhibit an almost linear evolution prior to the exhaustion of PO_4^{3-} and NO_3^- allowing the computation of mean TOC production rates. During this period, bacterial abundance was low and no phytoplankton species other than *E. huxleyi* were present in significant numbers (S. Jacquet, unpublished data, 2001), so TOC changes are mainly due to primary production by coccolithophorids. Likewise, since changes of PIC are linear from d₁₁ until the coccolithovirus passed a threshold value of about $5 \times 10^6 \text{ part. mL}^{-1}$, it is possible to compute the mean PIC production rates (Figure 7) prior to viral lysis.

[37] TOC increased steadily from d₁₀ to d₁₅ in all the mesocosms at rates ranging from 21.4 to 25.9 $\mu\text{molC kg}^{-1} \text{d}^{-1}$ (Figure 6). TOC production rates are similar under the three $p\text{CO}_2$ conditions (Figure 7). In contrast, the mean rate of PIC production (Figure 7) was conspicuously lower in the

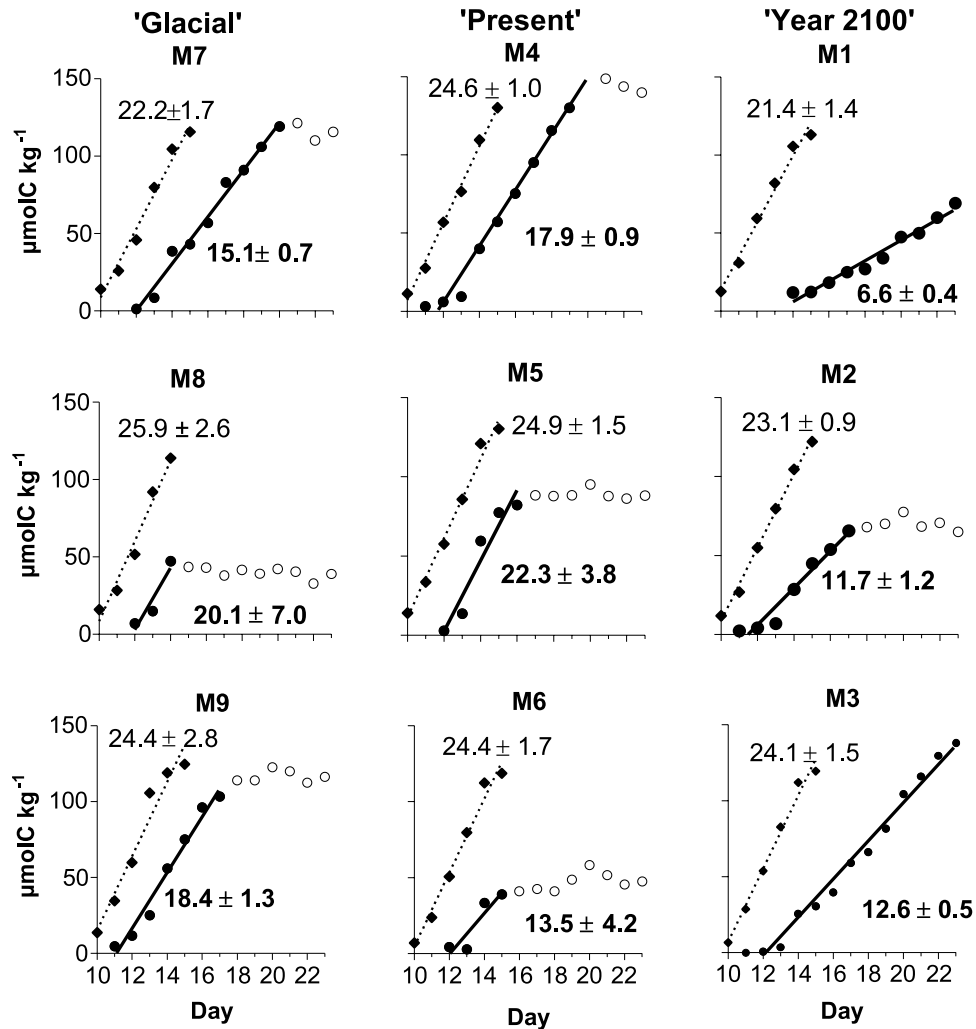


Figure 6. Changes in the standing stocks of total organic carbon (squares) from d_{10} until exhaustion of nutrients, with a regression line (dotted line) and corresponding slope and standard error (plain text), and particulate inorganic carbon between d_{11} to d_{23} (circles), with a regression line (thick line) and corresponding slope and standard error (bold text). Regression lines of particulate inorganic carbon were computed prior to viral lysis ($EhV < 5 \cdot 10^6$ part. mL⁻¹, solid circles).

year 2100 conditions (10.3 ± 3.2 µmol C kg⁻¹ d⁻¹) than in the present (17.9 ± 4.4 µmol C kg⁻¹ d⁻¹) and in the glacial (17.9 ± 2.5 µmol C kg⁻¹ d⁻¹) conditions. The mean PIC/TOC production ratio (C:P ratio) of *E. huxleyi* is similar in the glacial and present conditions between 0.73 and 0.78, but fell to 0.45 in the year 2100 conditions.

3.7. Carbon Losses

[38] Carbon losses were calculated as the difference between TOC produced by photosynthesis (estimated from the integration of NCP_{DIC}) and the accumulation of POC in the water column (data from Engel *et al.* [2004a]). Carbon losses during the peak of the bloom were conspicuously higher in the year 2100 (48 ± 10 µmol C kg⁻¹ d⁻¹) than under the glacial conditions (25 ± 16 µmol C kg⁻¹ d⁻¹) while TOC production remained similar (Figure 7). If integrated over the d_1 – d_{15} period, this trend is enhanced, carbon losses being more than twice as high in the year

2100 (74 ± 14 , µmol C kg⁻¹ d⁻¹) than under glacial conditions (34 ± 16 µmol C kg⁻¹ d⁻¹) (data not shown).

4. Discussion

4.1. The $p\text{CO}_2$ Changes and Buffering Effect of the Carbonate System

[39] Until d_{14} , changes in DIC_{31} followed the same trend and the same magnitude in all mesocosms while changes in $p\text{CO}_2$ were conspicuously different between the three conditions right from the beginning of the experiment (Figure 1). Indeed, the magnitude of changes in $p\text{CO}_2$ from d_0 to d_{14} was 6 times higher in the year 2100 conditions than in the glacial conditions, while until d_{14} , differences in DIC_{31} patterns between mesocosms were not significant since NCP_{DIC} was roughly similar under the three $p\text{CO}_2$ conditions and NCC was negligible. Therefore differences in the magnitudes of $p\text{CO}_2$ changes with regard to the $p\text{CO}_2$

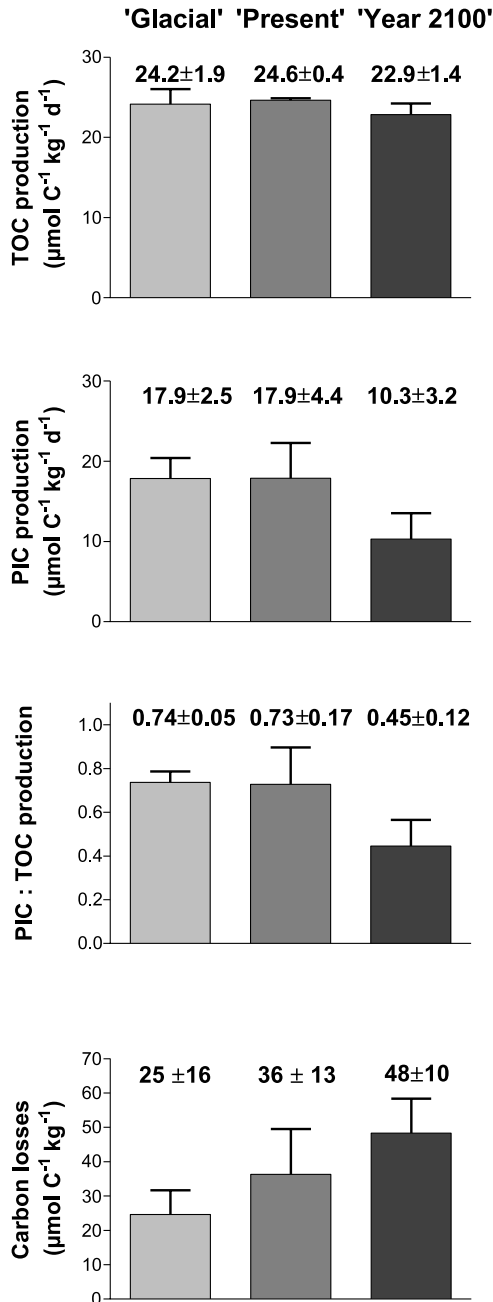


Figure 7. Mean and standard deviation of total organic carbon (TOC) production between d_{10} and d_{15} (before nutrient depletion), mean particulate inorganic carbon (PIC) production from d_{11} until viral lysis, mean PIC production:mean TOC production ratio (C:P), and carbon losses for the three $p\text{CO}_2$ conditions (light shading, glacial; dark shading, present; black, year 2100).

conditions are not ascribable to biological processes and must be explained taking into account the buffering effect of the carbonate system.

[40] The chemical buffer factor ($\beta = \Delta p\text{CO}_2 / \Delta \text{DIC}$) describes the change in $p\text{CO}_2$ relative to the DIC change induced by an input/output of dissolved CO_2 . It results from equilibrium dissociation reactions of the carbonate system

and is a function of several physico-chemical conditions, among them on the $p\text{CO}_2$ itself. The evolution of the buffer factor, calculated for the initial conditions of the experiment, is given in Figure 8. The β increases from 9.6 in the glacial conditions to 16.6 in the year 2100 conditions. Subsequently, for the same removal of CO_2 by primary production, the consequent decrease of $p\text{CO}_2$ is 6 times higher in the year 2100 condition ($\Delta p\text{CO}_2 = 116 \text{ ppmV}$ for $\Delta \text{DIC} = 20 \mu\text{mol kg}^{-1}$ and $\beta = 16.6$ at $p\text{CO}_2 = 700 \text{ ppmV}$, and $\text{DIC} = 2000 \mu\text{mol kg}^{-1}$) than under the glacial conditions ($\Delta p\text{CO}_2 = 20 \text{ ppmV}$ for $\Delta \text{DIC} = 20 \mu\text{mol kg}^{-1}$ and $\beta = 9.6$ at $p\text{CO}_2 = 180 \text{ ppmV}$ and $\text{DIC} = 1740 \mu\text{mol kg}^{-1}$).

[41] Thus, owing to thermodynamic interactions of the carbonate system, the change in $p\text{CO}_2$ is significantly higher in the year 2100 condition than in the other conditions, even though the process originally responsible of these $p\text{CO}_2$ changes, i.e., the uptake of CO_2 by photosynthesis, appears to be roughly similar under the three $p\text{CO}_2$ conditions. Hence one can note that in the future CO_2 rich world, other processes, such as temperature oscillations, upwelling of CO_2 rich waters, or precipitation of calcium carbonate [Frankignoulle et al., 1994] among others, will also contribute to the thermodynamic enhancement of the amplitude of $p\text{CO}_2$ changes from daily to seasonal timescales. In the same way, a higher spatial heterogeneity of $p\text{CO}_2$ can be expected from local to global scales.

[42] At the end of the experiment, from d_{16} onward, $p\text{CO}_2$ remained constant or slightly increased whereas DIC_{31} continued to decrease in most mesocosms. The decoupling of $p\text{CO}_2$ and DIC_{31} , associated to a decrease of TA_{31} , indicates the larger influence of NCC compared to NCP on $p\text{CO}_2$ as observed in natural coccolithophorid blooms and mesocosm experiments [Robertson et al., 1994; Purdie and Finch, 1994; Buitenhuis et al., 1996].

4.2. Primary Production and Carbon Export

[43] The effect of $p\text{CO}_2$ on growth, productivity and calcification of the coccolithophorid *E. huxleyi* is still a matter of debate. In our study, no conspicuous changes in primary productivity (both NCPy_{O_2} and $\text{NPPy}_{14\text{C}}$) related to $p\text{CO}_2$ conditions were observed during the peak of the *E. huxleyi* bloom. Differences in the NCP and NPP ob-

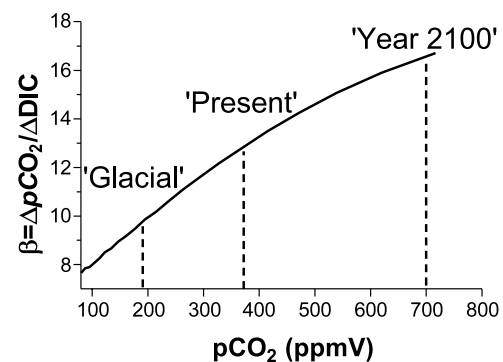


Figure 8. Buffer factor of the carbonate system for increasing partial pressure of CO_2 at the initial conditions of the experiment (salinity, 31.3; temperature, 10.0°C; TA , 2150 $\mu\text{mol kg}^{-1}$).

Table 2. Changes in CaCO_3 Production, Organic Carbon Production, and C:P Ratio of *Emiliana huxleyi* With Increasing $p\text{CO}_2$ Reported in Literature^a

	<i>E. huxleyi</i> Strain	Nitrate Concentration, $\mu\text{mol L}^{-1}$	Irradiance, $\mu\text{mol m}^{-2} \text{s}^{-1}$	Organic Production	CaCO_3 Production	C:P Ratio
Riebesell et al. [2000]	subarctic North Pacific natural assemblages	in situ conditions	30% of surface irradiance	0[–]	–	–
Zondervan et al. [2002]	Plymouth	100	150 (24/0), 150 (16/8)	+	–	–
after Riebesell et al. [2000]	Marine	100	80 (24/0)	+	–	–
and Zondervan et al. [2001]	Laboratory	100	30 (24/0) and 80 (16/8)	+	0	–
	B92/11A	100	15 (24/0)	0	0	0[–]
Sciandra et al. [2003]	Caen University TW1	0.5	170 (24/0)	–	–	0
This study	Norwegian natural assemblages	0.3 to 10	150 to 650 (16/8)	0	–	–

^aIn the irradiance column, numbers in brackets denote the daily light/day period in hours. Here “+”, “–”, and “0” denote, respectively, increase, decrease, and no significant changes, while brackets denote a trend not statistically significant. We limit our comparison to experiments which addressed the response of *E. huxleyi* to increase of $p\text{CO}_2$ or $[\text{CO}_2]$ and the concomitant decrease of the calcite saturation state (Ω_{calc}), within ranges of similar magnitude as predicted changes during the next hundred years.

served during the bloom decline should be ascribed to the occurrence or not of viral lysis rather than to some $p\text{CO}_2$ related effects.

[44] On the other hand, evidence of a higher loss of particulate organic carbon from the water column under year 2100 conditions (Figure 7) emerges surprisingly. Since DOC concentrations were similar under all $p\text{CO}_2$ conditions [Rochelle-Newall et al., 2004], while grazing was negligible, enhanced carbon losses observed under year 2100 conditions are likely due to a higher rate of particle settling. In fact, when normalized to *E. huxleyi* cell concentration, TEP production was highest under year 2100 conditions [Engel et al., 2004a], consistent with previous observations of enhanced TEP formation under elevated CO_2 [Engel, 2002]. TEP formation is typically seen as the result of carbon overproduction leading to exudation of polysaccharides by algal cells [Passow, 2002]. Aggregation of dissolved polysaccharides through a cascade of aggregation processes from the molecular scale up to the size of fast settling particles can lead to an enhancement of particle aggregation and subsequent export [Engel et al., 2004b]. The possible involvement of carbon-rich TEP as a mediator of enhanced particle settling in the year 2100 mesocosms is further supported by higher C:N ratio of suspended particles under high CO_2 conditions [Engel et al., 2004a].

4.3. Overview of the Response of the C:P Ratio to Rising CO_2

[45] In contrast to NCP_{DIC} , NCC exhibited a conspicuous decrease with increasing $p\text{CO}_2$. These responses lead to a drastic decrease of the PIC/TOC production ratio (C:P ratio) under elevated $p\text{CO}_2$. Also, calcification is delayed in the year 2100 condition, acting to reduce the overall amount of CaCO_3 produced during the experiment.

[46] During the pre-bloom period (d_0 to d_{10}) and the peak of the bloom (d_{10} to d_{15}), NO_3^- and PO_4^{3-} decreased rapidly from about $10 \mu\text{mol L}^{-1}$ and $0.7 \mu\text{mol L}^{-1}$, respectively, on d_{10} to below $0.4 \mu\text{mol L}^{-1}$ and $0.3 \mu\text{mol L}^{-1}$ on d_{15} with a mean photon flux density (PFD) around $650 \mu\text{mol m}^{-2} \text{s}^{-1}$ for 18:6 light period and a light attenuation coefficient at the bottom of the mesocosm (4 m) of about 80%. Therefore the mesocosms were not light limited but were in an intermediate state toward NO_3^- and PO_4^{3-} depletion. When attempt-

ing to reconcile the results of the present study to experiments reported in the literature and to draw a comprehensive picture of the response of primary production and calcification of *E. huxleyi* to elevated $p\text{CO}_2$, it is worth noting that the present knowledge is based on a mosaic of experiments with different growth conditions and involving several *E. huxleyi* ecotypes which give in some cases very different results (Table 2). However, it emerges that when irradiance is not drastically reduced [Zondervan et al., 2002], elevated $p\text{CO}_2$ appears to be detrimental to calcification [Riebesell et al., 2000; Zondervan et al., 2001, 2002; Sciandra et al., 2003] (also this study), [Riebesell et al., 2000; Zondervan et al., 2001; Zondervan et al., 2002; Sciandra et al., 2003] and this generally leads to a decrease of the C:P ratio (Table 2). Such response of calcification to changes in seawater carbonate chemistry has also been observed in corals and foraminifera [Gattuso et al., 1998; Wolf-Gladrow et al., 1999; Langdon et al., 2000; Leclercq et al., 2002; Langdon et al., 2003; Reynaud et al., 2003]. The cause of such a decrease of calcification by *E. huxleyi* in response to elevated $p\text{CO}_2$ remains unclear. If it can be almost intuitive that a decrease of Ω_{calc} concomitant to an increase of oceanic $p\text{CO}_2$ can reduce biogenic calcification, i.e., an environmental control of the calcification as it has been reported for corals reefs, some authors have rather suggested an internal control of calcification by *E. huxleyi*. For instance, several studies have suggested that calcification could support photosynthesis [Sikes et al., 1980; Nimer and Merrett, 1992; Anning et al., 1996; Buitenhuis et al., 1999], acting as an effective low-cost energy pathway to directly supply the chloroplast with CO_2 in addition to direct CO_2 diffusion into the cell, and then raise the concentration of CO_2 in the chloroplast at the site of photosynthesis. However, recent studies have severely questioned this hypothesis [Sekino and Shiraiwa 1994; Herfort et al., 2002, 2004; Rost and Riebesell, 2004]. Some other metabolic benefits from calcification have been suggested like the “trash-can” function facilitating the use of HCO_3^- in photosynthesis (see Paasche [2002] and Rost and Riebesell [2004] for reviews) and serving to remove excess Ca^{2+} [Berry et al., 2002]. Furthermore, calcification could rid the cell of excess energy and therefore prevent damage of the photosynthetic machinery [Rost and Riebesell, 2004].

[47] Some ecological implications have been also proposed. Hence coccolith production could protect the integrity of the cell and maintain a suitable environment around the cell surface [Young, 1994; Paasche, 2002]. However, among these ecological benefits, the ability of coccospheres to prevent viral lysis [Young, 1994] is not supported by our experiment. Indeed coccolithoviruses were detected in the course of the exponential growth phase in seven of the nine mesocosms, but virus-induced lysis was not detected in the two mesocosms where calcification rates were the lowest (M1 and M3: year 2100 conditions). Thus the benefits of calcification for coccolithophores still remain an open question.

[48] Published data on the effect of elevated CO_2 on organic carbon production and C:P ratio by *E. huxleyi* are even less clear (Table 2). Some papers report a decline of primary production at elevated $p\text{CO}_2$ and others an increase, while no conspicuous change was observed in the present study. It is obvious that environmental parameters such as light and nutrients interact with $p\text{CO}_2$ since they play a major role in the energy status and/or metabolism. Furthermore, two experiments carried out in similar conditions can show opposite trends regarding changes of POC and PIC production with $p\text{CO}_2$ [Nimer and Merrett, 1992; Buitenhuis et al., 1999] depending on the strain used. This underlines that attention must be paid to the ecotypes used in experiments or encountered in natural assemblages as also noted in a recent review on *E. huxleyi* physiology [Paasche, 2002].

[49] Among this mosaic of contrasting results, it must be pointed out that the two experiments carried out with natural communities under irradiance and nutrient concentrations close to environmentally realistic conditions [Riebesell et al., 2000] (and the present study) [Riebesell et al., 2000] converge to show that PIC production and the C:P ratio decrease markedly while POC production remains roughly constant with rising $p\text{CO}_2$.

[50] Previous experiments were carried out in batch or continuous cultures and provide little information on the dynamics of calcification in natural conditions. Following the development and decline of a bloom demonstrates that the onset of calcification was delayed by 24 to 48 hours in the year 2100 compared to glacial CO_2 conditions. Unfortunately, since the bloom prematurely collapsed owing to a massive viral infection, it is not possible to assess the overall duration of the calcification phase. However, we surmise that the delay in the onset of calcification under high $p\text{CO}_2$ could act to decrease the overall duration of the calcification phase. Such a reduction would lower the overall production of CaCO_3 in the full course of a coccolithophorid bloom.

4.4. Implications of the Observed $p\text{CO}_2$ Related Effects on Biogeochemical Fluxes

[51] The net effect of reduced calcification on air-sea CO_2 gradients and fluxes is the balance between two counter-acting processes. First, the decrease in calcification reduces CO_2 release. Second, the changes in seawater carbonate chemistry induced by rising $p\text{CO}_2$ lead to an increase of the molar ratio of released CO_2 over calcium carbonate

precipitation [Frankignoulle et al., 1995]. These two antagonistic processes seem to be balanced in coral reefs [Gattuso et al., 1999], but Zondervan et al. [2001] suggested that the response of pelagic calcification leans toward a negative feedback that increases the retention of CO_2 in the ocean. However, the response of pelagic biogenic CaCO_3 fluxes to rising CO_2 also needs to consider export processes. Blooms of *E. huxleyi* may be more efficient carbon sinks than other phytoplankton blooms as a result of the higher density of sedimenting cells and zooplankton fecal pellets, due to the high density of calcite [Buitenhuis et al., 2001]. This is supported by the compilation of sediment trap data below 1000 m depth which shows that ballast minerals, and in particular calcium carbonate, drives the sinking of organic carbon to the deep ocean [Armstrong et al., 2001; Klaas and Archer, 2002]. Hence, a lower C:P ratio of coccolithophorids under year 2100 conditions could lead to a smaller ballast effect and to a subsequent reduction of carbon export, thereby acting as a positive feedback to rising atmospheric CO_2 .

[52] In the present study, however, we actually observed the opposite, since carbon export by the *E. huxleyi* community, estimated as carbon losses, was higher under year 2100 conditions. Enhancement of carbon export through TEP production conspicuously overcomes the diminution of the ballast effect and turns the overall response of export of *E. huxleyi* to rising CO_2 concentration toward a negative feedback. This comes in addition to the decrease of the production of CO_2 as a consequence of the reduction of both rate and duration of calcification. Finally, if the enhancement of carbon export driven by higher TEP production under elevated $p\text{CO}_2$ is as significant for other phytoplanktonic groups as for coccolithophorids, then it would potentially represent a major negative feedback on rising atmospheric CO_2 .

5. Conclusions

[53] No conspicuous change of both net community productivity and net primary productivity of *E. huxleyi* was detected during the peak and the decline of a bloom of the coccolithophorid *E. huxleyi* for $p\text{CO}_2$ ranging from 175 to 600 ppmV. In contrast, the rate of net community calcification declined at elevated $p\text{CO}_2$, corroborating the observations of Riebesell et al. [2000], Zondervan et al. [2001, 2002], and Sciandra et al. [2003] on cultures of *E. huxleyi*. Furthermore, the onset of calcification is delayed by 24 to 48 hours in the year 2100 conditions compared to glacial conditions. The decrease of calcification rate combined with a rather constant organic carbon production led to a significant decrease of the C:P ratio.

[54] When comparing previous reports on the response of organic and inorganic carbon production of *E. huxleyi* to increasing $p\text{CO}_2$, it appears that in nonsaturating light and nutrient replete conditions, the increase in $p\text{CO}_2$ promotes organic carbon production [Riebesell et al., 2000; Zondervan et al., 2001, 2002] unless $p\text{CO}_2$ becomes too high (above 1000 ppmV) [Nimer et al., 1994]. In contrast, under nutrient-limiting conditions, organic carbon production remains constant [Riebesell et al., 2000] (also the

present study) or even decreases [Sciandra et al., 2003] with increasing $p\text{CO}_2$.

[55] Since the changes of both organic and CaCO_3 production with rising $p\text{CO}_2$ are strongly influenced by light and nutrient conditions as well as by the level of $p\text{CO}_2$, one could expect even more complex response of the C:P ratio. On the whole, a decrease of the C:P ratio with increasing $p\text{CO}_2$ appears to be a general trend with the exceptions under severe light or nutrient limitations. However, it must be pointed out that in most studies, little attention has been paid to the ecotype of *E. huxleyi* or to species other than *E. huxleyi*. Information available to date [Zondervan et al., 2001, 2002] indicates differential responses depending on the species considered. Also, the interaction of increased temperature, which is significant in corals [Reynaud et al., 2003], has not been investigated in coccolithophorids. Any prediction of the future response of ocean biogeochemistry to elevated $p\text{CO}_2$ must therefore take into consideration the composition of the community as well as the interaction with various other environmental parameters which are also predicted to change. In this sense, it is relevant to note that increased surface temperature will lead to a higher stratification and lower nutrient inputs, so that the evolution of marine communities and ecosystems should be envisaged in a “high CO_2 , low nutrient and warmer ocean” context.

[56] Many open questions need to be settled to predict reliably the response of coccolithophorids to rising CO_2 . However, it is worth noting that the two experiments carried out in environmentally realistic conditions converge satisfactorily and suggest that organic carbon production remains roughly constant with rising CO_2 while inorganic carbon production decreases drastically, reducing concomitantly the C:P production. Moreover, a delay in the onset of calcification under elevated $p\text{CO}_2$ conditions superimposed on a decrease of CaCO_3 production rate is likely to reduce the overall production of CaCO_3 in the course of a coccolithophorid bloom.

[57] **Acknowledgments.** This work is dedicated to our invaluable colleagues and friends Roland Wollast and Michel Frankignoulle who left us on 28 July 2004 and 13 March 2005, respectively. We are grateful to Anja Engel, Emma Rochelle-Newall, and Antoine Sciandra for fruitful discussions, to Marie-Dominique Pizay for technical assistance, to Jorun Egge for her welcome at the marine biological station of the University of Bergen, and to Daniel Delille and two anonymous reviewers for their pertinent comments on the manuscript. Access to installations from the University of Bergen was funded by the Improving Human Potential Programme from the European Union (contract HPRI-CT-1999-00056 “Bergen Marine”). A. V. B. and M. F. were, respectively, a post-doctoral researcher and a senior research associate at the Fonds National de la Recherche Scientifique. B. D. and J. H. were supported by the Belgian Federal Office for Scientific, Technical and Cultural Affairs (contracts EV/12/7E and EV/11/5A, respectively). This is MARE contribution 062.

References

- Anderson, L. G., C. Haraldson, and R. Lindegren (1992), Gran linearization of potentiometric Winkler titration, *Mar. Chem.*, **37**, 179–190.
- Anning, T., N. Nimer, M. J. Merrett, and C. Brownlee (1996), Costs and benefits of calcification in coccolithophorids, *J. Mar. Syst.*, **9**, 45–56.
- Armstrong, R. A., C. Lee, J. I. Hedges, S. Honjo, and S. G. Wakeham (2001), A new, mechanistic model for organic carbon fluxes in the ocean based on the quantitative association of POC with ballast minerals, *Deep Sea Res., Part II*, **49**, 219–236.
- Berry, L., A. R. Taylor, U. Lucken, K. P. Ryan, and C. Brownlee (2002), Calcification and inorganic carbon acquisition in coccolithophores, *Funct. Plant. Biol.*, **29**, 289–299.
- Bijma, J., H. J. Spero, and D. W. Lea (1999), Reassessing foraminiferal stable isotope geochemistry: Impact of the oceanic carbonate system (experimental results), in *Use of Proxies in Paleoceanography: Examples From the South Atlantic*, edited by G. Fischer and G. Wefer, pp. 489–512, Springer, New York.
- Bratbak, G., W. Wilson, and M. Heldal (1996), Viral control of *Emiliania huxleyi* blooms?, *J. Mar. Syst.*, **9**, 75–81.
- Buitenhuis, E. T., J. Van Bleijswijk, D. Bakker, and M. Veldhuis (1996), Trends in inorganic and organic carbon in a bloom of *Emiliania huxleyi* in the North Sea, *Mar. Ecol. Prog. Ser.*, **143**, 271–282.
- Buitenhuis, E. T., H. J. W. De Baar, and M. J. W. Veldhuis (1999), Photosynthesis and calcification by *Emiliania huxleyi* (Prymnesiophyceae) as a function of inorganic carbon species, *J. Phycol.*, **35**, 949–959.
- Buitenhuis, E. T., P. Van der Wal, and H. J. W. De Baar (2001), Blooms of *Emiliania huxleyi* are sinks of atmospheric carbon dioxide: A field and mesocosm study derived simulation, *Global Biogeochem. Cycles*, **15**(3), 577–587.
- Castberg, T., A. Larsen, R. A. Sandaa, C. P. D. Brussaard, J. K. Egge, M. Heldal, R. Thyrhaug, E. J. van Hannen, and G. Bratbak (2001), Microbial population dynamics and diversity during a bloom of the marine coccolithophorid *Emiliania huxleyi* (Haptophyta), *Mar. Ecol. Prog. Ser.*, **221**, 39–46.
- Chen, C. Y., and E. G. Durbin (1994), Effects of pH on the growth and carbon uptake of marine phytoplankton, *Mar. Ecol. Prog. Ser.*, **109**, 83–94.
- Dickson, A. G. (1990), Thermodynamics of the dissociation of boric acid in synthetic seawater from 273.15 to 318.15 K, *Deep Sea Res., Part A*, **37**, 755–766.
- Dong, L. F., N. A. Nimer, E. Okus, and M. J. Merrett (1993), Dissolved inorganic carbon utilization in relation to calcite production in *Emiliania huxleyi* (Lohmann) Kamptner, *New Phytol.*, **123**, 679–684.
- Engel, A. (2002), Direct relationship between CO_2 uptake and transparent exopolymer particles production in natural phytoplankton, *J. Plankton Res.*, **24**, 49–53.
- Engel, A., et al. (2004a), Testing the direct effect of CO_2 concentration on marine phytoplankton: A mesocosm experiment with the coccolithophorid *Emiliania huxleyi*, *Limnol. Oceanogr.*, **50**, 493–507.
- Engel, A., U. Thoms, U. Riebesell, E. Rochelle-Newall, and I. Zondervan (2004b), Polysaccharide aggregation as a potential sink of marine dissolved organic carbon, *Nature*, **428**, 929–932.
- Frankignoulle, M. (1994), A complete set of buffer factors for acid/base CO_2 system in seawater, *J. Mar. Syst.*, **5**, 111–118.
- Frankignoulle, M., C. Canon, and J.-P. Gattuso (1994), Marine calcification as a source of carbon dioxide: Positive feedback to increasing atmospheric CO_2 , *Limnol. Oceanogr.*, **39**, 458–462.
- Frankignoulle, M., M. Pichon, and J.-P. Gattuso (1995), Aquatic calcification as a source of carbon dioxide, in *Carbon Sequestration in the Biosphere*, edited by M. Beran, pp. 265–271, Springer, New York.
- Frankignoulle, M., A. V. Borges, and R. Biondo (2001), A new design of equilibrator to monitor carbon dioxide in highly dynamic and turbid environments, *Water Res.*, **35**, 1344–1347.
- Gao, K., Y. Aruga, K. Asada, and M. Kiyohara (1993), Influence of enhanced CO_2 on growth and photosynthesis of the red algae *Gracilaria* sp and *G-chilensis*, *J. Appl. Phycol.*, **5**, 563–571.
- Gattuso, J.-P., M. Frankignoulle, I. Bourge, S. Romaine, and R. W. Buddemeier (1998), Effect of calcium carbonate saturation of seawater on coral calcification, *Global Planet. Change*, **18**, 37–46.
- Gattuso, J.-P., D. Allemand, and M. Frankignoulle (1999), Photosynthesis and calcification at cellular, organismal and community levels in coral reefs: A review on interactions and control by carbonate chemistry, *Am. Zool.*, **39**, 160–183.
- Gran, G. (1952), Determination of the equivalence point in potentiometric titration, part II, *Analyst*, **77**, 661–671.
- Hedges, J. I., J. A. Baldock, Y. Gélinas, C. Lee, M. L. Peterson, and S. G. Wakeham (2002), The biochemical and elemental compositions of marine plankton: A NMR perspective, *Mar. Chem.*, **78**, 47–63.
- Herfort, L., B. Thake, and J. Roberts (2002), Acquisition and use of bicarbonate by *Emiliania huxleyi*, *New Phytol.*, **156**, 427–436.
- Herfort, L., E. Loste, F. Meldrum, and B. Thake (2004), Structural and physiological effects of calcium and magnesium in *Emiliania huxleyi* (Lohmann) Hay and Mohler, *J. Struct. Biol.*, **148**, 307–314.
- Hiwatari, T., A. Yuzawa, M. Okazaki, M. Yamamoto, T. Akano, and M. Kiyohara (1995), Effects of CO_2 concentrations on growth in the coccolithophorids (haptophyta), *Energy Convers. Manage.*, **36**, 779–782.
- Hoover, T. E., and D. C. Berkshire (1969), Effects of hydration in carbon dioxide exchange across an air-water interface, *J. Geophys. Res.*, **74**, 456–464.

- Jacquet, S., M. Heldal, D. Iglesias-Rodriguez, A. Larsen, W. Wilson, and G. Bratbak (2002), Flow cytometric analysis of an *Emiliana huxleyi* bloom terminated by viral infection, *Aquat. Microb. Ecol.*, *27*, 111–124.
- Jähne, B., G. Heinz, and W. Dietrich (1987), Measurement of the diffusion coefficients of sparingly soluble gases in water, *J. Geophys. Res.*, *92*, 10,767–10,776.
- Klaas, C., and D. E. Archer (2002), Association of sinking organic matter with various types of mineral ballast in the deep sea: Implications for the rain ratio, *Global Biogeochem. Cycles*, *16*(4), 1116, doi:10.1029/2001GB001765.
- Knap, A. H., A. Michaels, H. Close, H. W. Ducklow, and A. G. Dickson (Eds.) (1994), Protocols for the Joint Global Ocean Flux Study (JGOFS) core measurements, *JGOFS Rep. 19*, 170 pp., Carbon Dioxide Inf. Anal. Cent., Oak Ridge Natl. Lab., Oak Ridge, Tenn.
- Langdon, C., T. Takahashi, C. Sweeney, D. Chipman, J. Goddard, F. Marubini, H. Aceves, H. Barnett, and M. J. Atkinson (2000), Effect of calcium carbonate saturation state on the calcification rate of an experimental coral reef, *Global Biogeochem. Cycles*, *14*(2), 639–654.
- Langdon, C., W. S. Broecker, D. E. Hammond, E. Glenn, K. Fitzsimmons, S. G. Nelson, T. H. Peng, I. Hajdas, and G. Bonani (2003), Effect of elevated CO_2 on the community metabolism of an experimental coral reef, *Global Biogeochem. Cycles*, *17*(1), 1011, doi:10.1029/2002GB001941.
- Leclercq, N., J.-P. Gattuso, and J. Jaubert (2002), Primary production, respiration, and calcification of a coral reef mesocosm under increased CO_2 partial pressure, *Limnol. Oceanogr.*, *47*, 558–564.
- Lewis, E., and D. W. R. Wallace (1998), Program Developed for CO_2 System Calculations, *Rep. ORNL/CDIAC-105*, Carbon Dioxide Inf. Anal. Cent., Oak Ridge Natl. Lab., Oak Ridge, Tenn.
- Marie, D., C. P. D. Brussaard, R. Thyrhaug, G. Bratbak, and D. Vault (1999), Enumeration of marine viruses in culture and natural samples by flow cytometry, *Appl. Environ. Microbiol.*, *65*, 45–52.
- Milliman, J. D., P. J. Troy, W. M. Balch, A. K. Adams, Y.-H. Li, and F. T. Mackenzie (1999), Biologically mediated dissolution of calcium carbonate above the chemical lysocline?, *Deep Sea Res., Part I*, *46*, 1653–1669.
- Nimer, N., and M. J. Merrett (1992), Calcification and utilization of inorganic carbon by the coccolithophorid *Emiliana huxleyi* (Lohmann), *New Phytol.*, *121*, 173–177.
- Nimer, N. A., and M. J. Merrett (1993), Calcification rate in *Emiliana huxleyi* Lohmann in response to light, nitrate and availability of inorganic carbon, *New Phytol.*, *123*, 673–677.
- Nimer, N. A., C. Brownlee, and M. J. Merrett (1994), Carbon dioxide availability, intracellular pH and growth-rate of the coccolithophore *Emiliana huxleyi*, *Mar. Ecol. Prog. Ser.*, *109*, 257–262.
- Paasche, E. (2002), A review of the coccolithophorid *Emiliana huxleyi* (Prymnesiophyceae) with particular reference to growth, coccolith formation, and calcification-photosynthesis interactions, *Phycologia*, *40*, 503–529.
- Passow, U. (2002), Transparent exopolymer particles (TEP) in aquatic environments, *Prog. Oceanogr.*, *55*, 287–333.
- Purdie, D. A., and M. S. Finch (1994), Impact of a coccolithophorid bloom on dissolved carbon dioxide in sea water enclosures in a Norwegian fjord, *Sarsia*, *79*, 379–387.
- Qiu, B. S., and K. S. Gao (2002), Effects of CO_2 enrichment on the bloom-forming cyanobacterium *Microcystis aeruginosa* (Cyanophyceae): Physiological responses and relationships with the availability of dissolved inorganic carbon, *J. Phycol.*, *38*, 721–729.
- Redfield, A. C., B. H. Ketchum, and F. A. Richards (1963), The influence of organisms on the composition of sea-water, in *The Composition of Sea-Water and Comparative and Descriptive Oceanography*, edited by M. N. Hill, pp. 26–87, Wiley-Interscience, Hoboken, N. J.
- Reynaud, S., N. Leclercq, S. Romaine-Lioud, C. Ferrier-Pagès, J. Jaubert, and J.-P. Gattuso (2003), Interacting effects of CO_2 partial pressure and temperature on photosynthesis and calcification in a scleractinian coral, *Global Change Biol.*, *9*, 1660–1668.
- Richards, F. A. (1965), Anoxic basins and fjords, in *Chemical Oceanography*, vol. 1, edited by J. P. Riley and G. Skirrow, pp. 611–645, Elsevier, New York.
- Riebesell, U., D. A. Wolf-Gladrow, and V. Smetacek (1993), Carbon dioxide limitation of marine phytoplankton growth rates, *Nature*, *361*, 249–251.
- Riebesell, U., I. Zondervan, B. Rost, P. D. Tortell, R. Zeebe, and F. M. M. Morel (2000), Reduced calcification of marine plankton in response to increased atmospheric CO_2 , *Nature*, *407*, 364–367.
- Robertson, J. E., C. Robinson, D. R. Turner, P. Holligan, A. J. Watson, P. Boyd, E. Fernandez, and M. Finch (1994), The impact of a coccolithophore bloom on oceanic carbon uptake in the northeast Atlantic during summer 1991, *Deep Sea Res., Part I*, *41*, 297–314.
- Rochelle-Newall, E., B. Delille, M. Frankignoulle, J.-P. Gattuso, S. Jacquet, U. Riebesell, A. Terbruggen, and I. Zondervan (2004), Chromophoric dissolved organic matter in experimental mesocosms maintained under different $p\text{CO}_2$ levels, *Mar. Ecol. Prog. Ser.*, *272*, 25–31.
- Rost, B., and U. Riebesell (2004), Coccolithophores and the biological pump: Responses to environmental changes, in *Coccolithophores: From Molecular Processes to Global Impact*, edited by H. R. Thierstein and J. R. Young, pp. 99–125, Springer, New York.
- Roy, R., L. Roy, J. C. Vogel, C. Porter-Moore, T. Pearson, C. E. Good, F. J. Millero, and D. M. Campbell (1993), The dissociation constants of carbonic acid in seawater at salinities 5 to 45 and temperatures 0 to 45°C, *Mar. Chem.*, *44*, 249–267.
- Schroeder, D. C., J. Oke, G. Malin, and W. H. Wilson (2002), Coccolithovirus (Phycodnaviridae): Characterisation of a new large dsDNA algal virus that infects *Emiliana huxleyi*, *Arch. Virol.*, *147*, 1685–1698.
- Sciandra, A., J. Harlay, D. Lefèvre, R. Lemée, P. Rimmelin, M. Denis, and J.-P. Gattuso (2003), Response of coccolithophorid *Emiliana huxleyi* to elevated partial pressure of CO_2 under nitrogen limitation, *Mar. Ecol. Prog. Ser.*, *261*, 111–122.
- Sekino, K., and Y. Shiraiwa (1994), Accumulation and utilization of dissolved inorganic carbon by a marine unicellular coccolithophorid, *Emiliana-huxleyi*, *Plant Cell Physiol.*, *35*, 353–361.
- Sikes, C. S., R. D. Roer, and K. M. Wilbur (1980), Photosynthesis and coccolith formation: Inorganic carbon sources and net inorganic reaction of deposition, *Limnol. Oceanogr.*, *25*, 248–261.
- Smith, S. V. (1985), Physical, chemical and biological characteristics of CO_2 gas flux across the air-water interface, *Plant Cell Environ.*, *8*, 387–398.
- Uppström, L. (1974), The boron-chlorinity ratio of deep seawater from the Pacific Ocean, *Deep Sea Res. Oceanogr. Abstr.*, *21*, 161–163.
- Vault, D. (1989), CytoPC: Processing software for flow cytometric data, *Signal Noise*, *2*, 8.
- Weiss, R. F. (1974), Carbon dioxide in water and seawater: The solubility of a non-ideal gas, *Mar. Chem.*, *2*, 203–215.
- Wolf-Gladrow, D. A., U. Riebesell, S. Burkhardt, and J. Bijma (1999), Direct effects of CO_2 concentration on growth and isotopic composition of marine plankton, *Tellus, Ser. B*, *51*, 461–476.
- Young, J. R. (1994), Variation in *Emiliana huxleyi* coccolith morphology in samples from the Norwegian EHUX experiment, *Sarsia*, *79*, 417–425.
- Zimmerman, R. C., D. G. Kohrs, D. L. Steller, and R. S. Alberte (1997), Impacts of CO_2 enrichment on productivity and light requirements of eelgrass, *Plant Physiol.*, *115*, 599–607.
- Zondervan, I., R. E. Zeebe, B. Rost, and U. Riebesell (2001), Decreasing marine biogenic calcification: A negative feedback on rising atmospheric $p\text{CO}_2$, *Global Biogeochem. Cycles*, *15*(2), 507–516.
- Zondervan, I., B. Rost, and U. Riebesell (2002), Effect of CO_2 concentration on the PIC/POC ratio in the coccolithophore *Emiliana huxleyi* grown under light-limiting conditions and different daylengths, *J. Exp. Mar. Biol. Ecol.*, *272*, 55–70.

R. G. J. Bellerby, Bjerknes Centre for Climate Research, University of Bergen, Allégaten 55, N-5007 Bergen, Norway.

A. V. Borges and B. Delille, Unité d'Océanographie Chimique, MARE, Université de Liège, Allée du 6 août 17, B-4000 Liège, Belgium. (bruno.delille@ulg.ac.be)

L. Chou and J. Harlay, Laboratoire d'Océanographie Chimique et Géochimie des eaux, Université Libre de Bruxelles, Campus de la plaine, CP208, Boulevard du Triomphe, B-1050 Bruxelles, Belgium.

J.-P. Gattuso, Laboratoire d'Océanographie de Villefranche, UMR 7093 CNRS-Université de Paris 6, BP 28, F-06234 Villefranche-sur-mer, France.

S. Jacquet, Station INRA d'Hydrobiologie Lacustre, UMR 42 Cartell, CNRS, BP 511, F-74203 Thonon, France.

U. Riebesell, Leibniz Institute for Marine Sciences, University of Kiel, Duesternbrooker Weg 20, D-24105 Kiel, Germany.

I. Zondervan, Alfred Wegener Institute for Polar and Marine Research, P.O. Box 120161, D-27515 Bremerhaven, Germany.